Geomorphology 171–172 (2012) 83–93

Contents lists available at SciVerse ScienceDirect

Geomorphology

journal homepage: www.elsevier.com/locate/geomorph

Early Holocene (8.6 ka) rock avalanche deposits, Obernberg valley (Eastern Alps): Landform interpretation and kinematics of rapid mass movement

Marc Ostermann [a,*], Diethard Sanders [a], Susan Ivy-Ochs [b,c], Vasily Alfimov [c], Manfred Rockenschaub [d], Alexander Römer [d]

[a] Institute for Geology and Palaeontology, University of Innsbruck, A-6020 Innsbruck, Austria
[b] Department of Geography, University of Zurich, CH-8057 Zurich, Switzerland
[c] Laboratory of Ion Beam Physics, ETH Zurich, CH-8093 Zurich, Switzerland
[d] Geological Survey of Austria, A-1030 Vienna, Austria

ARTICLE INFO

Article history:
Received 31 December 2011
Received in revised form 27 March 2012
Accepted 8 May 2012
Available online 24 May 2012

Keywords:
Alps
Rock avalanche
Cosmic ray exposure dating
LIDAR interpretation
Electrical tomography
Rock avalanche kinematics

ABSTRACT

In the Obernberg valley, the Eastern Alps, landforms recently interpreted as moraines are re-interpreted as rock avalanche deposits. The catastrophic slope failure involved an initial rock volume of about 45 million m³, with a runout of 7.2 km over a total vertical distance of 1330 m (fahrböschung 10°). ^{36}Cl surface-exposure dating of boulders of the avalanche mass indicates an event age of 8.6 ± 0.6 ka. A ^{14}C age of 7785 ± 190 cal yr BP of a palaeosoil within an alluvial fan downlapping the rock avalanche is consistent with the event age. The distal 2 km of the rock-avalanche deposit is characterized by a highly regular array of transverse ridges that were previously interpreted as terminal moraines of Late-Glacial. 'Jigsaw-puzzle structure' of gravel to boulder-size clasts in the ridges and a matrix of cataclastic gouge indicate a rock avalanche origin. For a wide altitude range the avalanche deposit is preserved, and the event age of mass-wasting precludes both runout over glacial ice and subsequent glacial overprint. The regularly arrayed transverse ridges thus were formed during freezing of the rock avalanche deposits.

1. Introduction

Rockslides and rock avalanches include gravity-driven, rapid slope failures that are larger than about 10^5 to 10^6 m^3 in volume (Evans et al., 2006). Most rock avalanches post-dating the Last Glacial Maximum (LGM) in the Alps are readily recognized by their shape and size as well as by an extremely poorly sorted composition ranging from cataclastic gouge to megablocks (Pollet and Schneider, 2004; Crosta et al., 2007). At a few locations, however, the interpretation of landforms composed of very poorly sorted deposits remains controversial. For instance, transverse and lateral ridges of rock avalanches may appear similar to terminal and lateral moraines of glaciers. Diamicts of fine-grained matrix hosting polished and striated rock fragments may, either, represent basal till, or may form in rock avalanches. In addition, rock avalanches can flow out over long distances, which may promote confusion with glacial sediments (cf. Hewitt, 1999).

In the Obernberg valley, Austria, the character of a rock avalanche deposit led to diverse interpretations for more than a hundred years. In its distal part, which is about 2 km in length, the avalanche mass shows a regular arrangement of ridges and hillocks that are roughly transversal to valley axis. Frech (1903), who first investigated these deposits, interpreted their entirety as a rock avalanche. Paschinger (1953) agreed, but interpreted the ridges as a result of decay of underlying glacial ice. Later, based solely on the morphology of ridges and hillocks, the landforms were thought to be terminal moraines and kames (Magiera, 2000; Ebner et al., 2003; Wastl, 2007). Herein, we present a survey based on field investigations, volume estimation using airborne laser scanning image, a digital elevation model and electrical tomography, and proxy event ages produced by radiocarbon and cosmic ray-exposure dating. Our results indicate that the purported glacial landforms accumulated from a rock avalanche 8.6 ± 0.6 ka ago. We discuss: (a) a potential relation of rock avalanching with the 8.2-ka climatic phase in the Alps, and (b) the significance of transversal ridges with respect to rock avalanche kinematics.

2. The study area

The SW–NE trending Obernberg valley is a 9-km-long tributary of the Wipp valley, about 25 km south of Innsbruck (Fig. 1). Over most of its extent, the Wipp valley follows the Brenner extensional fault. The hangingwall of the Brenner fault consists of the Oetztal–Stubai basement complex with an overlying, parautochthonous Mesozoic succession and two superposed thrust nappes (Blaser and Steinach nappes); the footwall is comprised of variegated metamorphic successions of a different tectonostratigraphic unit (Fig. 1) (Fügenschuh

* Corresponding author. Tel.: +43 512 507 5684.
E-mail address: marc.ostermann@uibk.ac.at (M. Ostermann).

0169-555X/$ – see front matter © 2012 Elsevier B.V. All rights reserved.
doi:10.1016/j.geomorph.2012.05.006

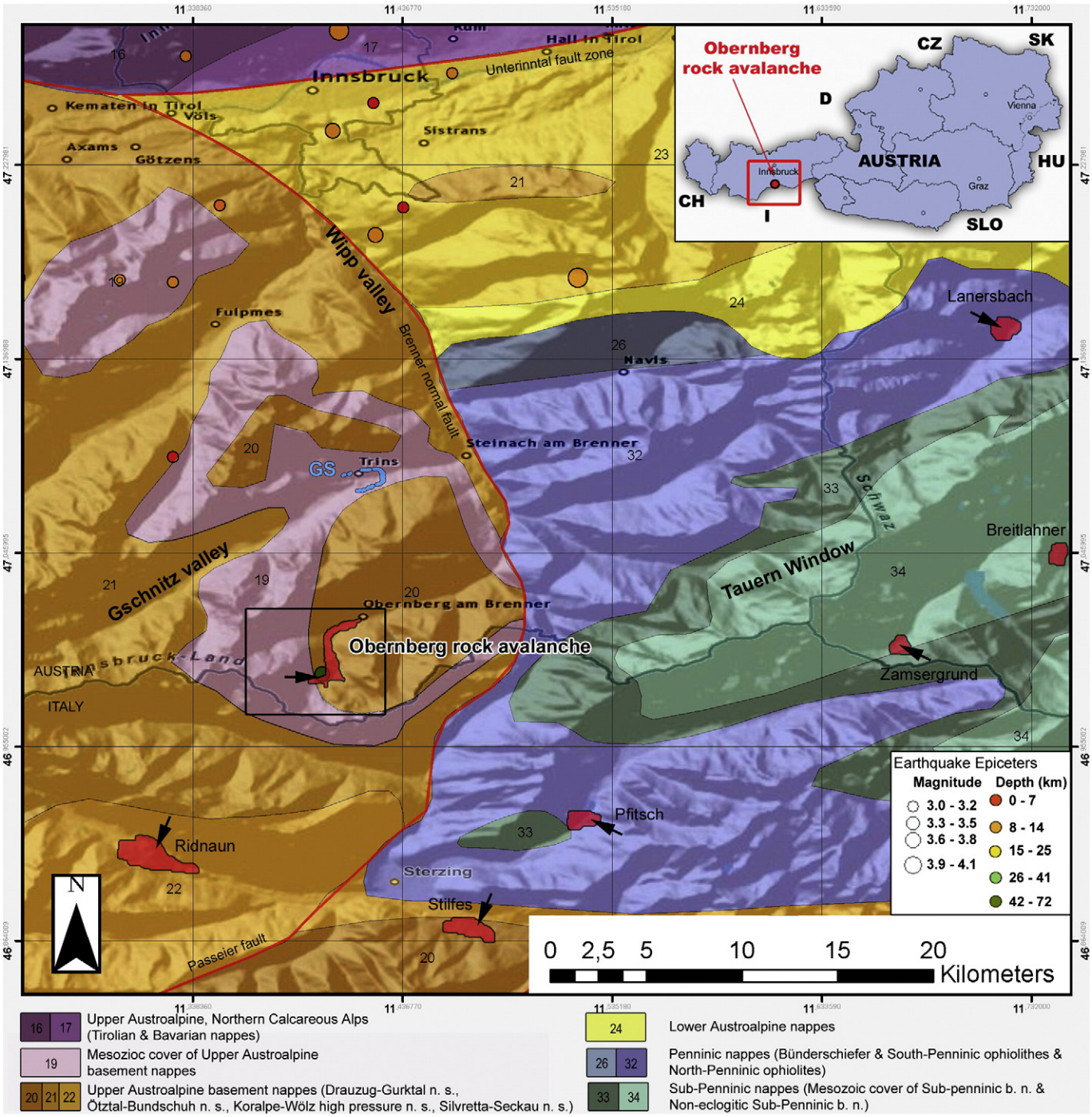

Fig. 1. The Obernberg rock avalanche and rockslides/rock avalanches (red areas) nearby, displayed on the tectonic map of Schmid et al. (2004), with a digital elevation model in the background. Earthquakes in this region according to the NEIC dataset (http://earthquake.usgs.gov/earthquakes) are indicated with multicolored and multi-sized dots. Dot size corresponds to earthquake magnitude, and dot color corresponds to the depth of the epicenters. GS: Gschnitz Stadial locus typicus.

et al., 1997). Neogene fission-track cooling ages in the footwall adjacent to the Brenner fault, and fault plane solutions of historical earthquakes suggest that the Brenner fault may still be active at a low rate (cf. Fügenschuh et al., 1997, 2000; Fügenschuh and Mancktelow, 2003; Reiter et al., 2003). The Obernberg rock avalanche detached from an isoclinally folded, Mesozoic series of calcitic to dolomitic marbles, calcitic phyllites and, subordinately, phyllites and quartzites (Fig. 2) (Rockenschaub et al., 2003). The dip/dip azimuth of schistosity in the isoclinally-folded series ranges from horizontal to 270–320°/10–20° (Reiser et al., 2010). The detachment scarp of the rock avalanche is located about 500 m west, and in the footwall of, an N–S striking normal fault (Portjoch fault) with a vertical throw of at least a few hundred meters. East of the Portjoch fault, the right flank of the See valley and that of the upper Obernberg valley consist mainly of quartz phyllite and mica schist of the Steinach nappe (Figs. 2 and 3). Whereas the mentioned Mesozoic series is deeply incised by many gullies, and the toes of slopes are covered with talus aprons, there is nearly no fluvial incision and talus formation within the Steinach nappe. The quartz phyllites there tend to form numerous slow moving, shallow to deep, mass movements (Fig. 3).

During the Last Glacial Maximum in the Eastern Alps (LGM, ca. 24–19 ka), the upper margin of glacial ice sloped from about

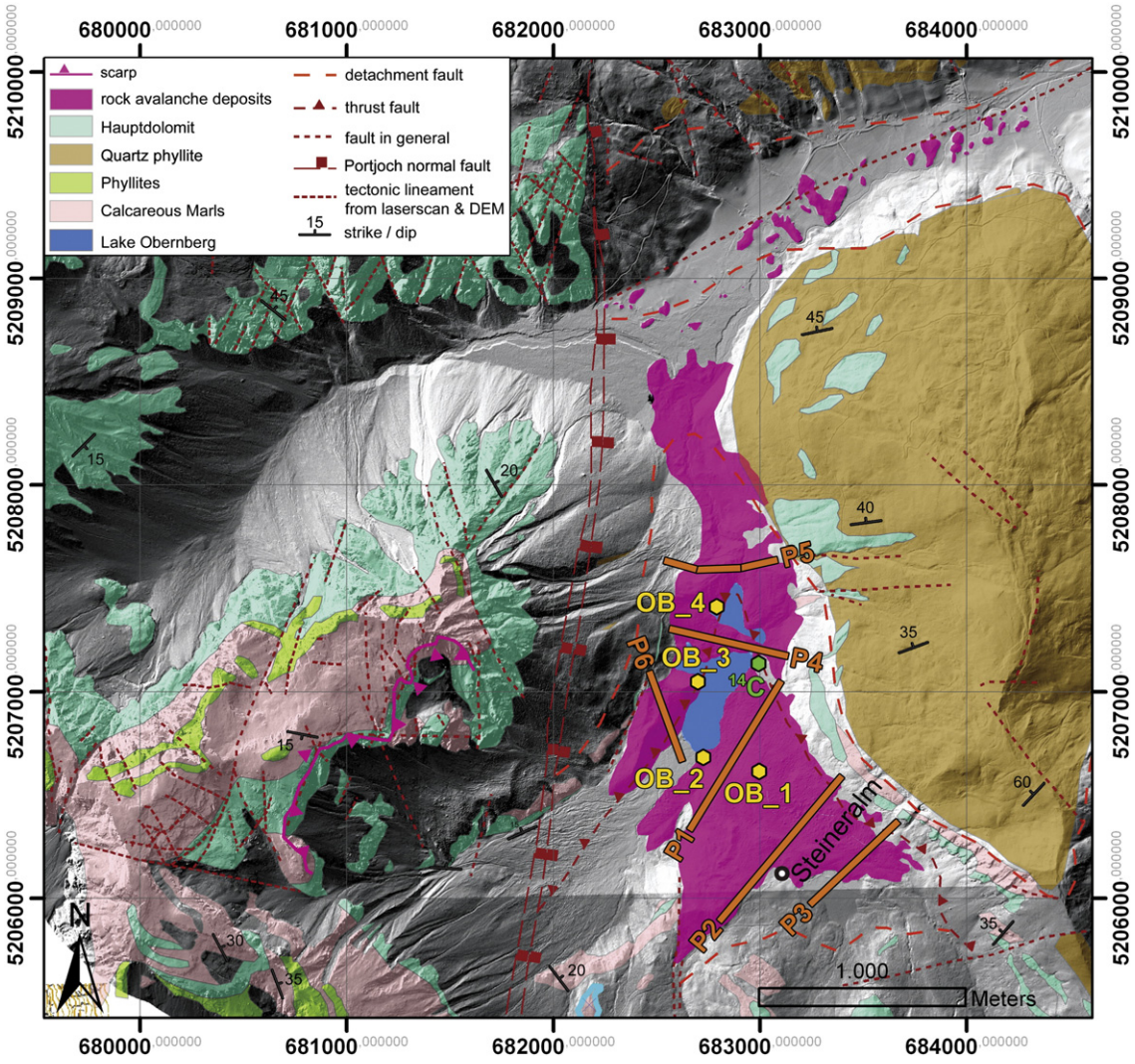

Fig. 2. Geological map of the Obernberg region (modified after Rockenschaub et al., 2003). The area is subdivided into two tectonic and lithological units by the Portjoch normal fault (PJ). Yellow circles: sampling sites for surface exposure dating. Green circle: sampling site for radiocarbon dating. Orange bars: geoelectric profiles P1 to P6 (see also Fig. 4).

2700 m a.s.l. in the heads of tributary valleys (Hinterenns and See valleys) to 2400 m a.s.l. in the central Obernberg valley; the summital Tribulaun range was a nunatak (Fig. 3) (Van Husen, 1987). In the Obernberg valley and its tributaries, the most widespread glacigenic sediment includes basal till and reworked basal till of the LGM. Subsequent to the LGM, after an early deglacial phase of rapid ice decay (Van Husen, 2004; Reitner, 2007), climatic amelioration and glacier shrinking were punctuated by stadials, that is, intermittent re-advances of valley glaciers (e.g. Kerschner, 1978; Van Husen, 1997; Ivy-Ochs et al., 2006). Along the northern (left) flank of the Obernberg valley, late-glacial ice-marginal deposits are preserved above the present valley floor, in an altitude range of 1820–1500 m a.s.l. These deposits may have accumulated during the Steinach Stadial, a phase of glacial re-advance older than $15{,}400 \pm 470$ ^{14}C yr BP (Magiera, 2000; Ivy-Ochs et al., 2006). In the neighboring Gschnitz valley, the type location of the Gschnitz Stadial, the terminal moraine complex is situated at the village Trins, at an elevation of 1410–1200 m a.s.l. (Fig. 1). The stabilization of the moraine complex has been attributed to no later than $15{,}400 \pm 1400$ years ago (Ivy-Ochs et al., 2006). In the Obernberg valley, probably as a result of a significantly smaller glacial catchment, no terminal moraine corresponding to the Gschnitz Stadial is present.

Lake Obernberg is situated on rock avalanche deposits (Fig. 3). The lake shows substantial seasonal and inter-annual variations in level, as a result of poor sealing of the lake basin combined with a high permeability of the underlying rock avalanche deposits. During low stage, the lake is separated into two parts (Reiser et al., 2010). The lake basin probably became deeper with time due to subsurface entrainment of fine-grained matrix in groundwater flow.

3. Methods

Field mapping was conducted on a scale of 1:5000 using topographic maps and laserscan images. High resolution airborne laserscan-data and a digital elevation model (DEM) with a 1-m resolution were provided by TIRIS (www.tirol.gv.at/). These data have been implemented into a GIS-system and combined with orthophotos (TIRIS, BEV), topographic maps (Österreichische Karte 1:50.000, BEV, Blatt 148 Brenner), and geological maps (Geological map of Austria, 1:50,000, Blatt 175 Sterzing; Geologisch-tektonische Karte der östlichen Stubaier Alpen, 1:25.000). The coordinate system and projection used are WGS1984 and UTM Zone 32N. Volume calculations and cross-sections were made with AutoCAD 2010.

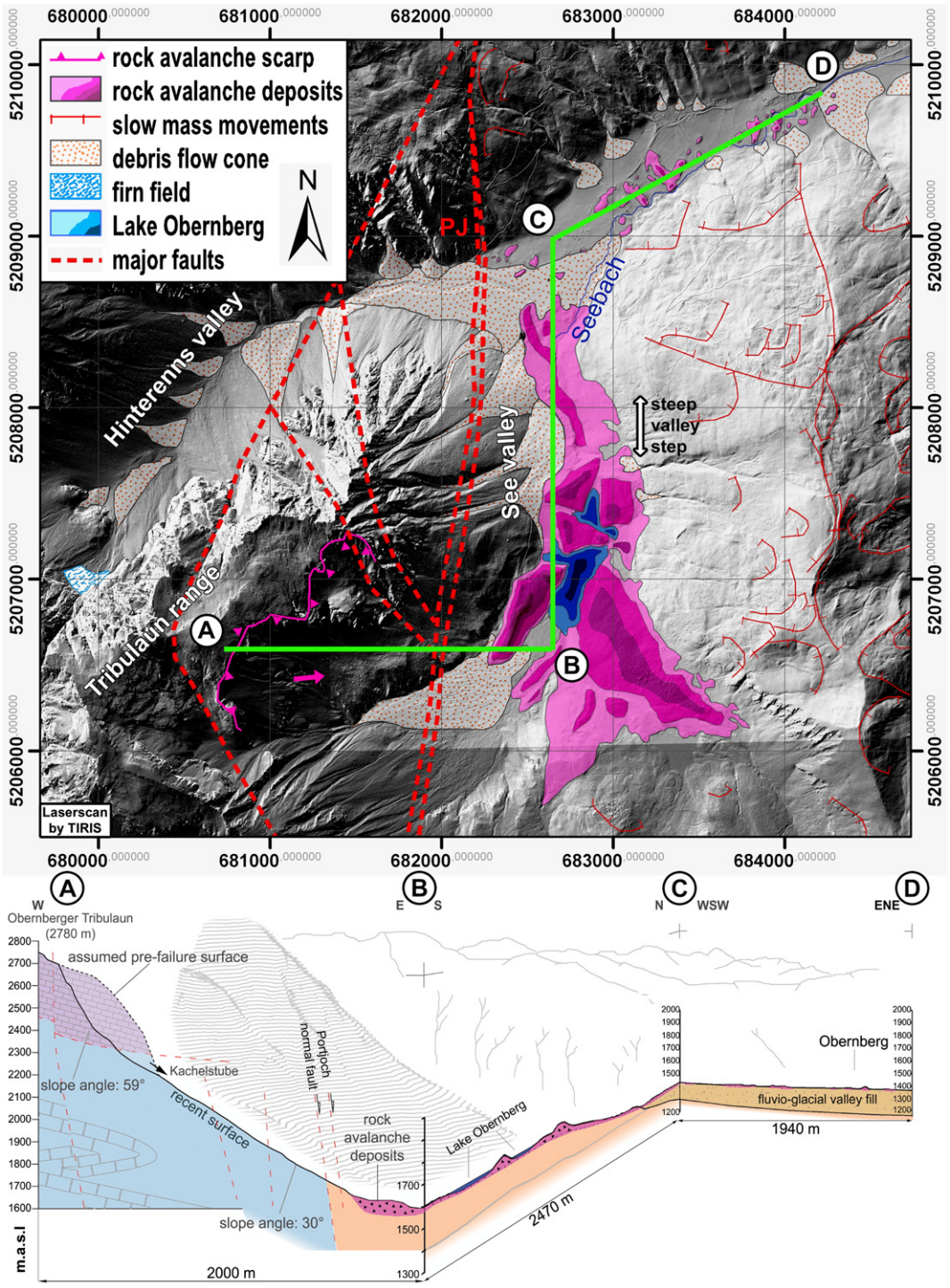

Fig. 3. Overview map of the Obernberg rock avalanche displayed on LIDAR-data (provided by TIRIS — Tyrolean spatial planning information system). The accumulation area has a color gradient displaying the estimated debris thickness distribution (light pink: 0–10 m; purple: 30–40 m). Lake Obernberg bathymetry is indicated in 5 m steps from pale blue to dark blue. Labeled white circles A to D denote areas motioned in the text. Green line from A (scarp area) to D (most distal part of the accumulation area): Cross-section shown in lower part of the figure.

For exposure dating with ^{36}Cl, near Lake Obernberg in the proximal sector of the rock avalanche, the surfaces of four boulders were sampled (locations shown in Fig. 2). Unfortunately, the distal sector of the avalanche deposit with transversal ridges (C–D in Fig. 3) is devoid of suitable boulders (those lying well above the enclosing sediment). Sample preparation is described in Ivy-Ochs et al. (2009). Approximately 60 g of rock was dissolved, after addition of 2.4 mg of ^{35}Cl carrier, with concentrated HNO_3. Cl was isolated and freed of S with several pH change steps and addition of $Ba(NO_3)_2$, respectively. ^{36}Cl and natural Cl (isotope dilution; Ivy-Ochs et al., 2004) were determined with accelerator mass spectrometry (Synal et al., 1997). Measured sample ^{36}Cl/Cl ratios were normalized to the ETH internal standard K382/4N with a value of $^{36}Cl/Cl = 1.736 \times 10^{-11}$ (normalized to the Nishiizumi standards in 2009) while the stable ^{37}Cl/^{35}Cl ratio was normalized to the natural $^{37}Cl/^{35}Cl$ ratio = 31.98% of the K382/4N standard and the machine blank. Measured sample ratios were also corrected for a procedural blank of 3×10^{-15}, which amounted to a correction of less than 2% for all samples. Major and trace element concentrations are given

in Table 1. Concentrations of B and Gd were below the detection limit. Exposure ages (Table 2) were calculated based on a sea level/high latitude production rate of 48.8 ± 1.7 atoms ^{36}Cl g(Ca)$^{-1}$ a^{-1} for production from spallation of Ca, and 5.3 ± 0.5 ^{36}Cl g(Ca)$^{-1}$ a^{-1} production due to muon capture on Ca (Stone et al., 1996, 1998) scaled after Stone (2000). Production of ^{36}Cl through low energy capture of thermal and epithermal neutrons is calculated following Liu et al. (1994) and Phillips et al. (2001) using a production constant of 760 ± 120 neutrons (g air)$^{-1}$ a^{-1} (Alfimov and Ivy-Ochs, 2009). Major element and samarium concentrations as well as major element concentrations (Table 1) were used to determine the fraction of low-energy neutrons available for capture by ^{35}Cl to form ^{36}Cl (Alfimov and Ivy-Ochs, 2009 and references therein). The contribution due to non-cosmogenic subsurface ^{36}Cl production calculated after Fabryka-Martin (1988) was negligible. Shielding corrections were done following Dunne et al. (1999). We used a rock density of 2.4 g cm^{-3}.

On the southern bank of Lake Obernberg, a paleosoil 1.2 m below the surface of a small alluvial fan was sampled for radiocarbon dating (Fig. 2). Radiocarbon ages (Table 3) were calibrated with OXCAL 4.0.1 (Bronk Ramsey, 2009) using the Int Cal 09 data set (Reimer et al., 2009).

In the proximal part of the rock avalanche deposit, six electrical tomographic profiles were made with a GEOMON4D resistivity meter, an in-house development of the Geological Survey of Austria, with a gradient electrode array configuration (Fig. 2; see Table 4 for key parameters of profiles). Data inversions were performed with the AGI EarthImager 2D software according to a robust inversion method based on an L2-norm criterion. The results of the inverted profiles are shown in Fig. 4 after suppressing aberrant resistivity values obtained due to bad coupling between electrodes and the sometimes rocky material.

4. Rock avalanche deposits

In the most proximal sector of the rock avalanche mass, a ridge up to 80 m in relief comprised of very poorly sorted bouldery sediment is present. Clasts of cobble to boulder size show in-situ fragmentation. Farther down, rock-avalanche deposits build lateral ridges along the Obernberg lakes. In addition, a continuous layer of bouldery deposit can be mapped for approximately 200 m in altitude onto the opposite, right-hand flank of the See valley (Fig. 3); the distribution of this deposit may suggest that it originated from a different mass-wasting event descended from the west-facing slope. The composition of clasts of folded marbles, however, indicates that it more likely derives from the detachment area of the Obernberg rock avalanche, i.e. from the eastern cliffs of the Tribulaun range. The medial part of the rock avalanche consists of a steeply sloping tongue of extremely-poorly sorted debris ranging up to boulders a few tens of meters in size (Figs. 3 and 5C). Finally, the distal part of the rock avalanche consists of a conspicuous array of hillocks and ridges that are described in more detail below (Figs. 3, 4 and 5).

Rock avalanche deposits exposed at the surface cover an area of ~1.9 km^2. Taking into account those parts of the avalanche that are buried by alluvial fans, talus slopes and colluvium, an area of ~3 km^2 was calculated (Abele, 1974: 2.7 km^2). The distance from the upper brink of the detachment scarp (2700 m a.s.l.) to the distal most toma hill (1370 m a.s.l.) is 7.2 km, yielding a fahrböschung angle of 10°. According to our calculation based on a digital elevation model, the total volume of rock avalanche deposits is 5.3 × 10^7 m³ (Paschinger, 1953: 5.7 × 10^7 m³). To reconstruct the rock volume detached from the scarp area (Fig. 3), we used a digital elevation model integrated with LIDAR data, aerial photos and topographic maps. The results give a maximum of close to 5.0 × 10^7 m^3 of rock before detachment (Paschinger, 1953: 5.6 × 10^7 m^3). This indicates a volume increase of 5.6% from rock to rock avalanche deposit, being higher than 1.2% of Paschinger (1953), but anomalously low relative to a volume increase of up to 25–30% reported for mass-wastings of carbonate rocks (Abele, 1974; Hungr and Evans, 2004). This may suggest that the initial volume was overestimated by isohypse fitting; a volume of ~4.0–4.5 × 10^7 m^3 seems more realistic. With this deduced volume and a reconstructed area of 3 km^2, the Obernberg rockslide lies within the range of volume/area ratio of other rockslides and rock avalanches; the same holds for the ratio of runout length to vertical drop versus volume (cf. Abele, 1974; Dade and Huppert, 1998).

A minimum-age constraint of the mass-wasting event was obtained by radiocarbon dating of organic remnants found in alluvial fan deposits on the top of the rock avalanche deposits (Fig. 2). Two samples were taken: (a) Vera — 4980 (OB-14C_2) represents a paleosoil 120 cm below the surface of the alluvial fan, and (b) Vera — 4979 (OB-14C_1) is a piece of wood from about 20 cm below the recent fan surface (Table 3). From ^{36}Cl surface exposure dating of four boulder surfaces, we obtained the following exposure ages: 9.16 ± 0.40 ka (OB1), 12.09 ± 0.55 ka (OB2), 8.24 ± 0.60 ka (OB3), and 8.32 ± 0.40 ka (OB4). The average age of 8.6 ± 0.6 ka indicates an early Holocene age for the rock avalanche event (Table 2). We attribute the outlier-age 12.09 ± 0.55 ka to inheritance which is often observed in rock avalanche boulders (Ivy-Ochs et al., 2009).

5. Transversal ridges and hillocks

The distal part of the rock avalanche between Untereinsalm (1540 m a.s.l.) and Obernberg Village (~1370 m a.s.l.) is characterized by an array of 40 hillocks and transversal ridges with up to 17 m in vertical relief (Figs. 3, 4 and 5). Because of the lack of both natural outcrops and drill logs, we could not establish whether the hillocks and ridges are contiguous with each other or rather represent isolated forms. For reasons discussed below, however, we assume that they are connected with each other in the subsurface. These ridges and hillocks were interpreted as terminal moraines and kames because of their morphology (Magiera, 2000; Ebner et al., 2003; Wastl, 2007).

Cross-sections based on a digital elevation model with 1-m resolution show that the transversal ridges are arranged into two 'domains' each about 750 m in length (Fig. 5). Each domain consists of nine ridges, with the highest in the central part and progressively lower and elongated ones towards the distal and proximal margins. Two artificial outcrops (Fig. 7), each a few meters in height and about 10 m in length, provide insight into the internal fabric of ridges. Both outcrops show that the ridges consist of angular fragments of sand- to boulder-size clasts in disordered fabric; no systematic vertical/lateral sorting, stratification, and preferred orientation of clasts were observed. The fabric ranges, in a patchy pattern, from clast-supported with sparse interstitial matrix of structureless carbonate gouge to

Table 1
Major element data for the analyzed samples (determined by XRF at XRAL, Ontario, Canada).

Boulder no.	Al_2O_3 wt. %	CaO wt. %	Cr_2O_3 wt. %	Fe_2O_3 wt. %	K_2O wt. %	MgO wt. %	MnO wt. %	Na_2O wt. %	P_2O_5 wt. %	SiO_2 wt. %	TiO_2 wt. %	Sum	LOI	Sm ppm	Th ppm	U ppm
OB1	0.1	53.3	0.01	0.01	0.02	0.59	0.01	0.01	0.01	0.21	0.01	97.8	43.5	0.2	0.5	0.32
OB2	5.0	39.0	0.02	1.82	1.08	1.28	0.05	0.50	0.05	19.60	0.230	100.3	31.7	2.4	3.0	1.46
OB3	0.2	33.1	0.02	0.15	0.03	19.2	0.01	0.01	0.01	0.41	0.01	99.1	45.9	0.4	0.1	0.50
OB4	0.4	46.8	0.01	0.24	0.12	8.04	0.03	0.01	0.01	1.12	0.020	100.5	43.7	0.4	0.1	0.50

Table 2
Results of ^{36}Cl surface exposure dating.

Boulder no.	Alt. [m]	Easting [UTM WGS84 Z 32N]	Northing [UTM WGS84 Z 32N]	Thickness [cm]	Shielding	^{36}Cl [10^5 atoms ^{36}Cl/g rock]	Cl [ppm]	Exposure age [kyr]
OB1	1651	682,923	5,206,460	2.5	0.95	7.27 ± 0.20	31.3 ± 0.1	9.16 ± 0.40
OB2	1606	682,781	5,206,752	1	0.97	7.06 ± 0.22	2.3 ± 0.1	12.09 ± 0.55
OB3	1616	682,702	5,207,178	2	0.96	5.57 ± 0.24	95.0 ± 1.5	8.24 ± 0.60
OB4	1610	682,799	5,207,329	1.5	0.97	5.66 ± 0.20	24.2 ± 0.7	8.32 ± 0.40

matrix-supported. Many clasts of coarse gravel- to boulder-size are fragmented in situ, with opposite fracture walls still fitting. Both the orientation and density of fractures are highly variable among and within individual clasts.

6. Interpretation of the ground electrical tomography

Six multielectrode profiles were measured to get more detailed information on the depth and internal structure of the rock avalanche deposits. The locations of the profiles (P1–P6) are indicated in Fig. 2. The results of the geoelectric inversion of multi-electrode data on the profiles are shown in Fig. 4. To make comparison and interpretation easier, all profiles are depicted with the same color bar.

P1 shows a relatively homogenous cover of rock avalanche debris, represented by high resistivity (>3000 Ω m, red color in Fig. 4), reaching a maximum thickness of about 60 m, with an average thickness of about 50 m. The high resistivity can be explained by its high porosity, which is implied by the accumulation of large blocks (typical size of a few m^3 scale). Below this surficial layer, resistivity decreases with depth, indicating finer and wetter material that could be the expression of increased matrix content and/or fluvio-glacial deposits (orange and yellow colors in Fig. 4). The bedrock is built up by quartz phyllite with an electr. resistivity around 500 Ω m (green color). In the NNE part of this profile, low electr. resistivities (<50 Ω m, blue color) can be explained by the occurrence of a fault-zone.

The rock debris cover at P2 reaches from about 20 m in the NE to a maximum extent of 45 m in the middle part of the profile. In the SW of the profile near Steineralm (1737 m a.s.l., Fig. 2) the bedrock (quartz phyllite) is at surface or below a very thin talus cover. Here a low resistivity zone can also be observed. This anomaly may be attributed to a technical reason: drainage pipe and power supply in the vicinity of Steineralm.

P3 is characterized by up to 40 m thick rock avalanche debris in the NE. In the SW, in contrast, it consists of near-surface bedrock as well as water-saturated fluvial deposits and peaty material.

P4 is situated along the "Maria am See" peninsula that divides the lake basin of Lake Obernberg into two parts. The situation here is more complex. The evaluation of the profile leads to the interpretation of a dry part and a water saturated part of the rock avalanche debris. The ridge consists of about 10–20 m unsaturated on top, and up to 20 m thick water saturated rock avalanche debris below. The bedrock is almost built up by quartz phyllite. Towards the NW, electric resistivity in the substratum increases (~1000 Ω m), indicating the transition to the carbonatic units in the W.

P5 is situated on top of the steep valley step, where the northern most lake basin is dammed by rock debris. In the East, rock avalanche material is covered by a small alluvial cone (up to ~6 m in thickness) fed from a gully. The rock avalanche debris here reaches a thickness of ~25 m. In the central part of the profile, the prominent low resistivity anomaly can be interpreted as a fault-zone. This zone indicates the boundary of the carbonate bedrock (yellow and orange colors in Fig. 4) in the W and the quartz phyllite (green color) in the E. The high resistivity in the NW could also indicate a glacial or fluvial channel filled with rock avalanche debris.

P6 crosses the up to 80 m high ridge developed along the SW bank of Lake Obernberg. The geoelectric survey clearly shows that the whole ridge is composed of rock avalanche debris. Toward the S of the profile one can see the water saturated part of the rock avalanche debris with aggradation deposits on the top, coming in from the S into the lake basin. The bedrock here has carbonatic lithologies.

7. Discussion

The kinematics of the Obernberg rock avalanche is described in chronological order from A to D (Figs. 2 and 6).

(A) After detachment of the main volume of rock, the rock mass ran down a rectilinear slope ~30° in gradinet and 1200 m in length (Fig. 6A). Immediately after the detachment, the rock mass perhaps was still more-or-less intact and moved as a rockslide. We assume, however, that during run-down on the slope, the rock mass disintegrated by dynamic fragmentation and progressively turned into a rock avalanche (Davies and McSaveney, 1999; Davies et al., 1999).

(B) The rock avalanche ran across the valley floor and up onto the opposite slope ~12° in gradinet (Fig. 6B). Near Steineralm (1767 m a.s.l.), the rock-avalanche deposit consists of: (a) a surficial veneer of boulders of Hauptdolomit, resting on (b) calcareous marbles; this reflects the vertical distribution of these two lithologies in the scarp area (see Fig. 3).

Transition from (B) to (C). After run-up of the frontal part of the rock avalanche onto the opposite slope, some of the swashed material may have flowed back (Fig. 6B); the following part of the moving rock avalanche bulged up, and was forced to swerve towards the N. As a result, longitudinal ridges and grooves formed in the marginal part of the avalanche. In addition, in flowing down the very steep upper part of the See valley, the rock avalanche probably gained kinetic energy again.

Table 3
Results of radiocarbon dating.

Sample	Alt. [m]	Easting	Northing	Material	^{14}C-age [kyr]	cal-Age [kyr]
Vera — 4980 OB_14C_2	1608	686,191	5,206,273	Paleosoil	6.98 ± 45 [BP]	7.79 ± 0.19
Vera — 4979 OB_14C_1	1608	686,191	5,206,273	Wood	0.12 ± 45 [BP]	Modern

Table 4
Key parameters of the electrical tomography.

Electrical tomography profile	Length [m]	Orientation (first to last electrode)	Elevation [m a.s.l.] (min. elv.–max. elv.)	Unit electrode spacing [m]	Horizontal scale pixels per unit spacing
P1	736	NNE–SSW	1612–1672	8.00	9.97
P2	690	NE–SW	1728–1750	7.50	19.99
P3	570	NE–SW	1751–1789	7.50	12.08
P4	532	WNW–ESE	1607–1625	7.00	12.03
P5	552	W–E	1581–1618	6.00	9.92
P6	460	NNW–SSE	1591–1650	5.00	9.85

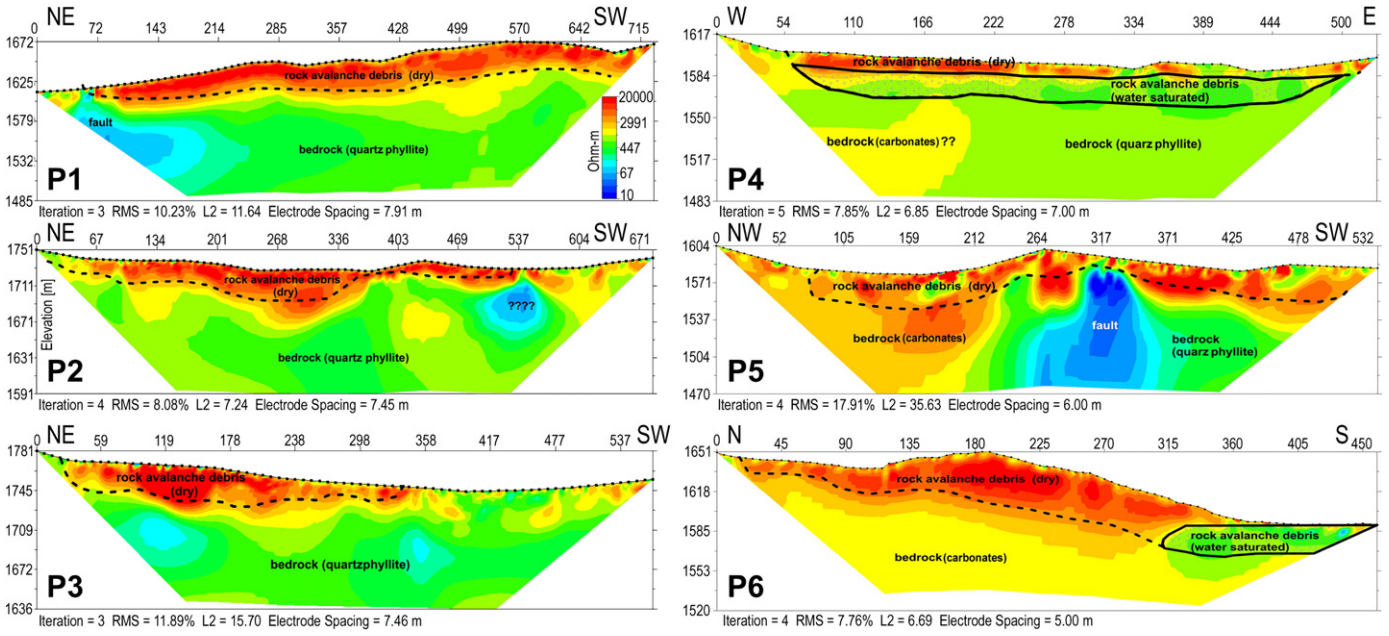

Fig. 4. Resistivity cross-sections (P1–P6) obtained by electrical tomography profiles (see Fig. 2). Values represented along the X-axis correspond to distance in meters form the starting point of the tomography profile. The Y-axis represents the elevation above sea level in meters. Parameters of each profile are given in Table 2.

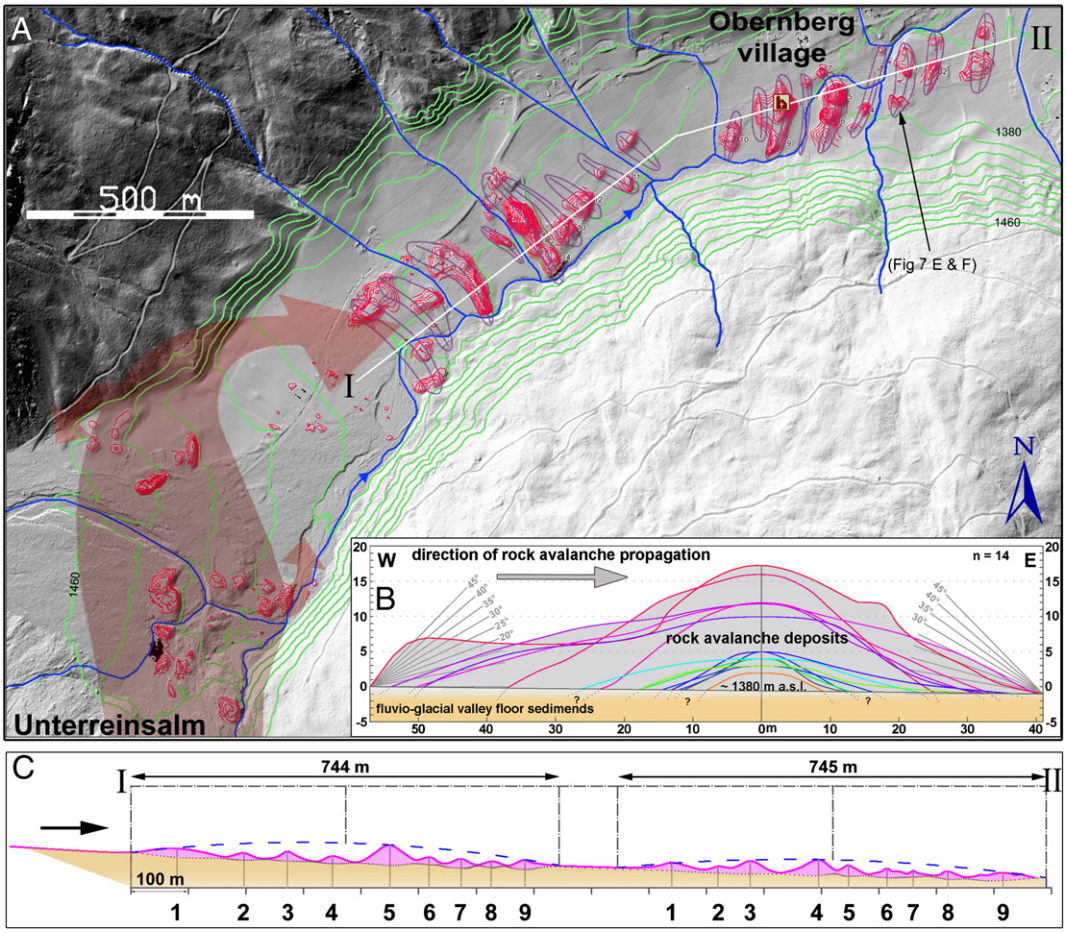

Fig. 5. Transversal ridges at Obernberg. A) Airborne laser scan image (by TIRIS) of the landscape at Obernberg. Red lines: 1-m contours for transversal ridges. Green lines: 10-m contours. B) Inset figure shows superposition of 14 cross-sections of transversal ridges. C) Cross-section from I to II (see A) through the transversal ridges, which show a very regular arrangement.

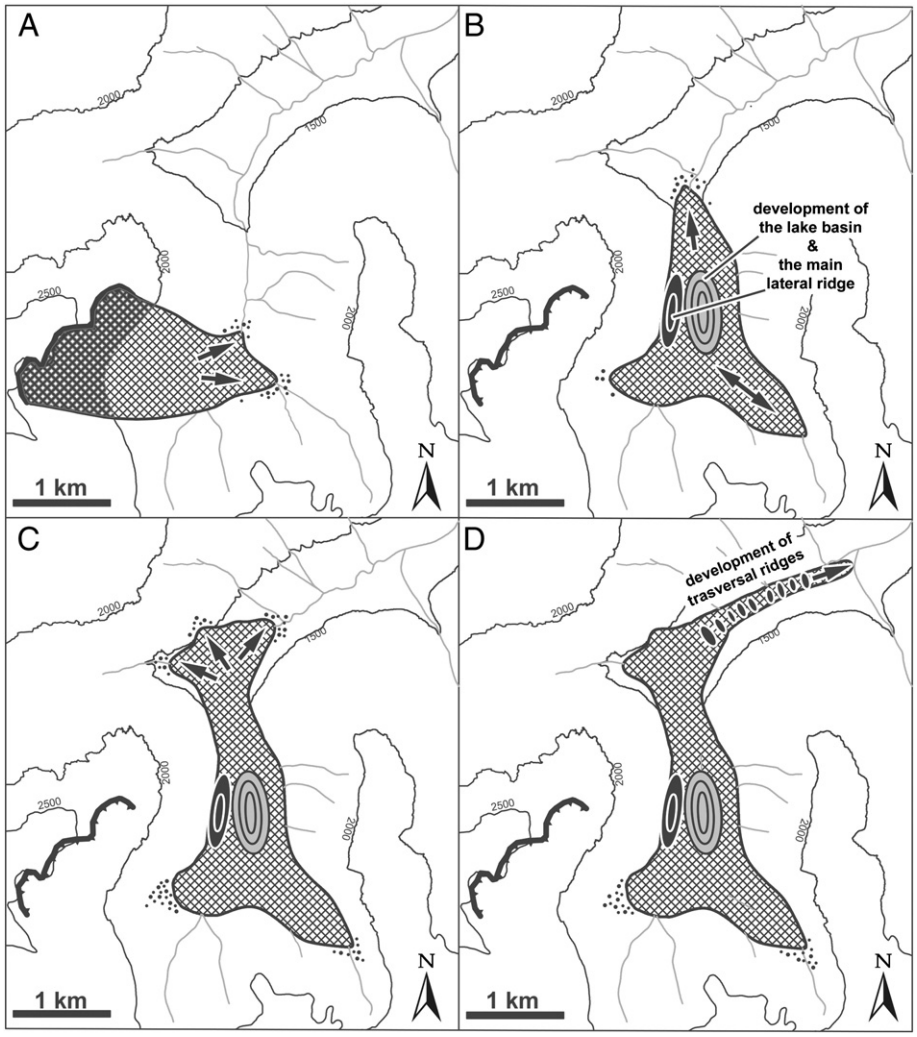

Fig. 6. Sketch maps of the propagation of the Obernberg rock avalanche (A to D). The closer hatch in A indicates the assumed former outline of the intact rock slope. Explanations are given in the text.

(C) When the rock avalanche ran up the northern slope of the Obernberg valley, a part of it branched off and ran up, for a limited distance, into the Hinterenns valley (Fig. 6C; see also Fig. 3, point C).

(D) The main body of the rock avalanche, however, continued to run down the Obernberg valley (Fig. 6D). There, kinetic energy dropped below the threshold for rock-avalanche movement, and the described arrays of transverse ridges formed.

Taking into account the velocities for rock avalanches from Zambrano (2008) and a runout distance of 7.2 km, we infer that the event happened within a time span of 0.8 to 2 min.

In the Alps, only a few mass-wasting events are dated into the range from ~9 to 7.5 ka. The age of 8.6 ± 0.6 ka of the Obernberg event may suggest a relation with the "8.2 ka cooling event" (cf. Rohling and Pälike, 2005). In the eastern part of the Eastern Alps, a cooling of ~3 °C into the 8.2 ka event needed 10–20 years, and cooler conditions then persisted from ~8.2 to 8.1 ka (Boch et al., 2009). The resolution of the numerical age of 8.6 ± 0.6 ka of the Obernberg rock avalanche event hence does not allow for an unequivocal correlation with the 8.2 ka cooling. In the eastern part of the Eastern Alps, there is no evidence for marked changes in seasonality or mean annual precipitation (Boch et al., 2009). Conversely, in the northern and western Alpine foreland, lake levels rose at about 8.2 kyr, probably due to increased precipitation and decreased summer temperatures (Magny et al., 2003). In NW-Germany, the onset of 8.2 ka event was characterized by a rapid switch to a phase of approximately 190 years of cooler and drier summers; similarly, winters were drier and cooler (Klitgaard-Kristensen et al., 1998; Prasad et al., 2009). If understood as a phase of cooler summers, the NW-Germany 8.2 ka event started between ~8.12 and 8.09 ka and ended at 7.93 ka (Prasad et al., 2009), i.e. nearly twice as long as in the eastern part of the Eastern Alps. This suggests that the response to the 8.2 ka event had a strong geographical component, provided that age assignments are sufficiently precise. Difficulties to capture the 8.2 ka event may also arise from the different methods of dating and the variegated records used (e.g., Alley and Ágústsdóttir, 2005; Kerschner et al., 2006; Prasad et al., 2009, and references therein). Because the climatic response of the central part of the western Eastern Alps to the 8.2 ka event is not documented to date, we thus refrain from suggesting a potential correlation of rock-avalanching with particular climatic conditions. In addition, only a minority of rockslides and rock avalanches of the Alps have been dated so far. This further impedes us to assess a potential correlation of palaeoclimate with catastrophic mass-wasting. In the Silvretta massif of the Central Alps, glaciers of N-facing cirques of the Kromer stadial (perhaps equivalent with the 8.2 ka phase) terminated at 2100 m a.s.l. or higher (Kerschner et al., 2006), i.e., in an altitude above the Obernberg rock-avalanche deposit. This further

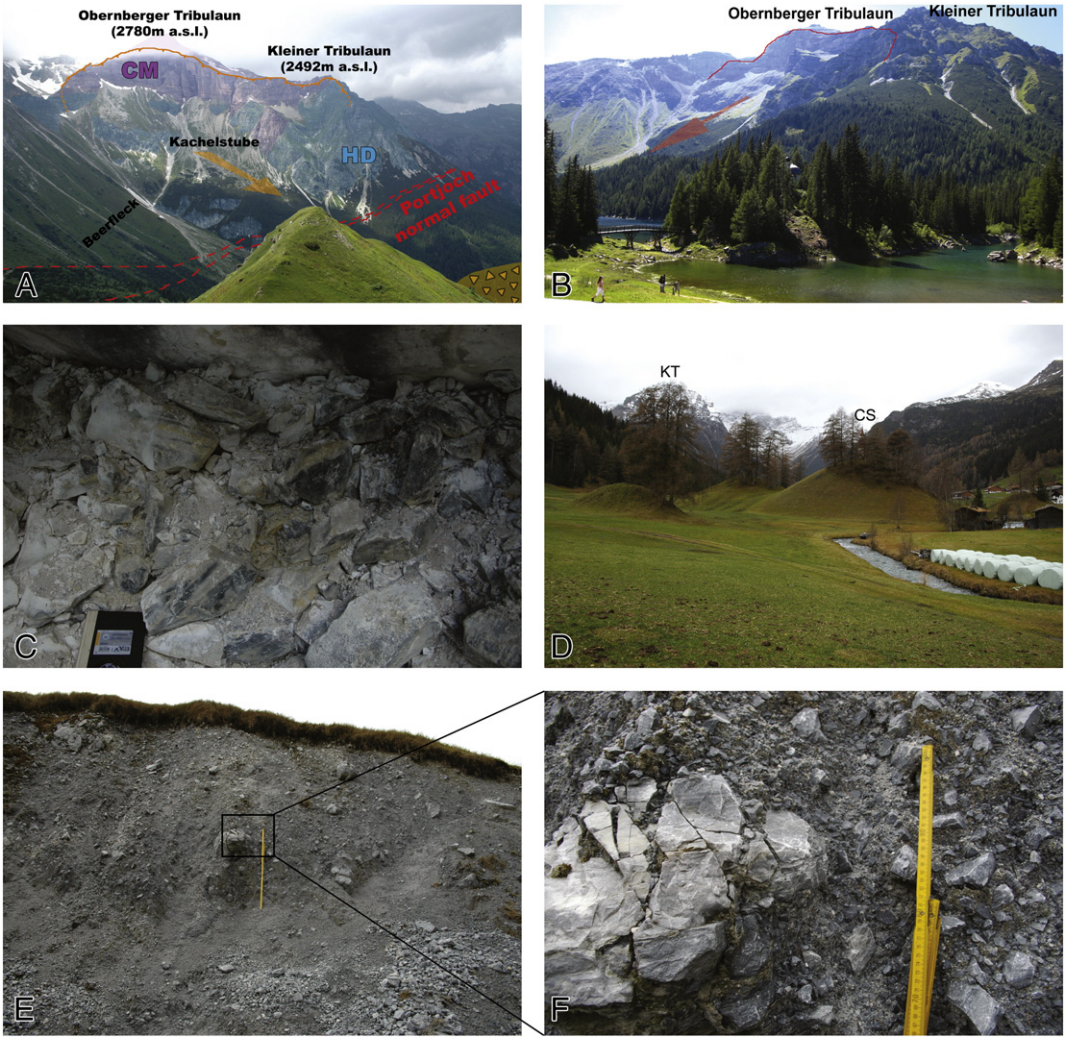

Fig. 7. Field photographs showing features related to the Obernberg rock avalanche. A) Overview of the scarp area of the Obernberg rock avalanche view towards W. The orange line represents the outline of the scarp. CM = calcareous marls, HD = Hauptdolomit. In the lower right corner rock avalanche debris is indicated in yellow. Notice the dissection of the upper part of the rock slope through faults and joints. B) Overview photo of Lake Obernberg with the northern lake basin in the foreground, view toward SW. The scarp area (red line) and the upper travel path (red arrow) in the background. Notice the big blocks in and around the lakes. Lake level is about 1.5 m below maximum. C) Chaotic fabric of angular clasts of calcareous marls and Hauptdolomit and fine grained matrix below a big block nearby the Lake Obernberg. Field book for scale. D) Hilly landscape at Obernberg view towards W. KT = Kleiner Tribulaun (2492 m a.s.l.). CS = church spire of the church of Obernberg situated on top of one of the transversal ridges. E) Artificial outcrop at one of the most distal transversal ridges. Angular clasts swimming in a fine grained matrix without any sorting. Stick = 1 m. F) Enlarged detail of E) showing a fractured clast of Hauptdolomit (jigsaw type). Visible stick = 44 cm.

suggests that the rock avalanche did not run out over a glacier. We also found no evidence that the avalanche deposit was overridden by a glacier.

Except for the present course of the Seebach stream (Fig. 3), the transverse ridges in the distal sector of the avalanche deposit were not dissected by fluvial activity. There is also no evidence for disintegration of the distal part of the avalanche mass by slow downslope movement after the event. Thus, at least the larger transverse ridges, as seen in Fig. 3, are well-preserved and in similar arrangement as they were immediately after the rock avalanching. However, smaller surface features such as scattered boulders or low ridges may have been removed upon agricultural amelioration for pasture. Compared with most other rock-avalanche masses in the Alps, the abundance and high regularity of the transversal ridges of the distal part of the Obernberg avalanche deposit are exceptional. The regularity may provide a record of the style of material movement (Fig. 6). The apparent excessive mobility of rock avalanches has been explained by sliding on, and/or lubrication of fine-grained deposits with incorporated snow, ice, and water (e.g., Abele, 1974; Goguel, 1978; Sartori et al., 2003; Hungr and Evans, 2004; De Blasio, 2009; Dufresne et al., 2010; Shugar and Clague, 2011). Another explanation for the high rock-avalanche mobility is based on the mechanics of the moving mass itself (e.g. Davies and McSaveney, 1999; Dufresne et al., 2010). Because a universal feature of large-volume catastrophic rock-slope failures is fragmentation (cf. Crosta et al., 2007), one key to the mobility of rock avalanches is comminution during downslope movement (Davies et al., 1999). Letting aside potential effects of snow or ice, or 'lubrication' by foreign materials, a rock mass probably moves as long as kinetic energy suffices to sustain dynamic fragmentation and resulting dilatancy by mutual particle impact (Imre et al., 2010). Propagation of kinetic energy may occur in acoustic waves that act to fluidize the moving particulate mass (Melosh, 1986; Collins and Melosh, 2003).

We infer that the distal-most transverse ridge of the Obernberg rock-avalanche mass was the first to freeze, and the more proximal ridges formed subsequently by successive upslope propagation of freezing. Each transverse ridge thus may represent the terminal record of some kind of wave or surge that traveled downslope. Surging, i.e., fluctuations of both velocity and thickness of a flow associated with downflow propagation of roll waves, is observed in fluid flows,

density flows, and debris flows of diverse compositions (e.g., Coussot and Meunier, 1996; Major, 1997; Balmforth and Mandre, 2004, and references therein). Roll waves do not require turbulence to develop, and can emerge also in granular flows (e.g., Daerr, 2001; Louge and Keast, 2001). Roll waves may overtake each other by run-up of faster surges into slower forerunners; overall, however, they strive towards quasi-periodic wave trains (all other conditions equal) (Forterre and Pouliquen, 2003). At least under certain experimental conditions, granular flows can evolve into a series of downslope-propagating roll waves pushing forward unmoved material resting in between the surges (Forterre and Pouliquen, 2003). No model of a granular flow undergoing dynamic disintegration, and explicitly treating the physical effects of disintegration from local scale up to the entire avalanche, exists as yet. Dynamic disintegration, perhaps the single most distinctive process in the movement of rock avalanches and rockslides, was analog modeled for a small volume of rock-like material in a centrifuge (Imre et al., 2010); however, this cannot reflect the potential behavior of a rock avalanche when in action as a whole over some period of time. Acoustic waves within rock fractures dissipate in areas close to the source (Melosh, 1996). In the distal part of a rock avalanche, acoustic waves from dynamic disintegration may become organized into downslope-propagating pulses, resulting in surging-style movement (cf. Collins and Melosh, 2003). The described transverse ridges thus may hint on the existence of surge-like flow behavior in the distal part of some rock avalanches.

8. Conclusions

(1) Surface exposure dating of boulders indicates that the Obernberg rock avalanche occurred 8570 ± 630 years ago; this age is supported by a ^{14}C age of 7785 ± 190 a cal BP of a palaeosol in alluvial fan deposits on the rock-avalanche deposits.
(2) The Obernberg rock avalanche is the first dated mass-wasting event in the Alps that potentially was associated with the 8.2 ka climatic cooling. The precise nature of the 8.2 ka event in the central part of the Eastern Alps, however, is insufficiently documented to sustain speculations on a triggering of the rock avalanche under a particular climatic condition.
(3) The distal 2 km of rock-avalanche deposits show an array of transverse ridges. These were previously interpreted as terminal moraines and kames. The internal fabric and nature of the sediment of the ridges are, however, incompatible with glacial moraines, but consistent with an origin from a rock avalanche.
(4) The transversal ridges are arranged into two highly regular higher-order waves, each of which consists of waxing and shrinking ridges. We suggest that the arrayed ridges reflect a mechanical aspect of the movement, perhaps propagation of waves towards the snout of the avalanche deposit.

Acknowledgments

This research was supported by the Austrian Science Fund FWF (P-20890-N10). Christoph Prager and Rainer Brandner are acknowledged for discussion. Special thanks to Alfred Gruber and Martin Reiser for providing the radiocarbon samples and to Hanns Kerschner for his general support. We also would like to thank Gerhard Bieber and Anna Ita for support at the geophysical survey, and the accelerator mass spectrometry group at Ion Beam Physics ETH Zurich for supporting labwork including ^{36}Cl AMS measurements.

Appendix A. Supplementary data

Supplementary data to this article can be found online at http://dx.doi.org/10.1016/j.geomorph.2012.05.006.

References

Abele, G., 1974. Bergstürze in den Alpen — ihre Verbreitung, Morphologie und Folgeerscheinungen: Wissenschaftliche Alpenvereinshefte, 25. 230 pp.
Alfimov, V., Ivy-Ochs, S., 2009. How well do we understand production of ^{36}Cl in limestone and dolomite? Quaternary Geochronology 4, 462–474.
Alley, R.B., Ágústsdóttir, A.M., 2005. The 8 k event and consequences of a major Holocene abrupt climate change. Quaternary Science Reviews 24, 1123–1149.
Balmforth, N.J., Mandre, S., 2004. Dynamics of roll waves. Journal of Fluid Mechanics 514, 1–33.
Boch, R., Spötl, C., Kramers, J., 2009. High-resolution isotope records of early Holocene rapid climate change from two coeval stalagmites of Katerloch Cave, Austria. Quaternary Science Reviews 28, 2527–2538.
Bronk Ramsey, C., 2009. Bayesian analysis of radiocarbon dates. Radiocarbon 51, 337–360.
Collins, G.S., Melosh, H.J., 2003. Acoustic fluidization and the extraordinary mobility of sturzstroms. Journal of Geophysical Research 108 (B10), 2473. http://dx.doi.org/10.1029/2003JB002465.
Coussot, P., Meunier, M., 1996. Recognition, classification and mechanical description of debris flows. Earth-Science Reviews 40, 209–227.
Crosta, G.B., Frattini, P., Fusi, N., 2007. Fragmentation in the Val Pola rock avalanche, Italian Alps. Journal of Geophysical Research 112, F01006. http://dx.doi.org/10.1029/2005JF000455.
Dade, W.B., Huppert, H.E., 1998. Long-runout rockfalls. Geology 26, 803–806.
Daerr, A., 2001. Dynamical equilibrium of avalanches on a rough plane. Physics of Fluids 13, 2115–2124.
Davies, T.R.H., McSaveney, M.J., 1999. Runout of dry granular avalanches. Canadian Geotechnical Journal 36 (2), 313–320.
Davies, T.R.H., McSaveney, M.J., Hodgson, K.A., 1999. A fragmentation-spreading model for long-runout rock avalanches. Canadian Geotechnical Journal 36, 1096–1110.
De Blasio, F.V., 2009. Rheology of a wet, fragmenting granular flow and the riddle of the anomalous friction of large rock avalanches. Granular Matter 11, 179–184.
Dufresne, A., Davies, T.R.H., McSaveney, M.J., 2010. Influence of runout-path material on emplacement of the Round Top rock avalanche, New Zealand. Earth Surface Processes and Landforms 35, 190–201.
Dunne, J., Elmore, D., Muzikar, P., 1999. Scaling factors for the rates of production of cosmogenic nuclides for geometric shielding and attenuation at depth on sloped surfaces. Geomorphology 27, 3–11.
Ebner, V., Edelmaier, F., Hofer, D., Hofer, M., Knor, N., Koch, J., Ortner, G., Renz, M., Ruf, P., Sacher, B., Van Asbroeck, P., Wanker, C., Wastl, M., 2003. Geologische Landesaufnahme, Kartenblätter GÖK 148 Brenner und GÖK 175 Sterzing — Erläuterungen zur Geomorphologie des hinteren Obernbergtals. In: Geologische Bundesanstalt (Ed.), Arbeitstagung der Geologischen Bundesanstalt "Brenner", Trins, Geologische Kartenblätter 148 Brenner und 175 Sterzing, pp. 209–215.
Landslides from massive rock slope failure. In: Evans, S.G., Scarascia Mugnozza, G., Strom, A.L., Hermanns, R.L. (Eds.), Proc. NATO Advanced Workshop, Celano, Italy, June 2002. : NATO Science Series: IV: Earth and Environmental Sciences, 49. Springer. 662 pp.
Fabryka-Martin, J.T., 1988. Production of radionuclides in the Earth and their hydrogeologic significance, with emphasis on chlorine-36 and iodine-129. Ph.D. thesis, Department of Hydrology and Water Resources, the University of Arizona.
Forterre, Y., Pouliquen, O., 2003. Long-surface-wave instability in dense granular flows. Journal of Fluid Mechanics 486, 21–50.
Frech, F., 1903. Über das Antlitz der Tiroler Zentralalpen. Zeitschr. d. D. u. Ö. a.-V. , pp. 1–31.
Fügenschuh, B., Mancktelow, N., 2003. Brennerabschiebung und Kinematik im Bereich der Periadriatischen Naht. In: Geologische Bundesanstalt (Ed.), Arbeitstagung der Geologischen Bundesanstalt "Brenner", Trins, Geologische Kartenblätter 148 Brenner und 175 Sterzing, pp. 125–126.
Fügenschuh, B., Seward, D., Mancktelow, N., 1997. Exhumation in a convergent orogen: the western Tauern window. Terra Nova 9, 213–217.
Fügenschuh, B., Mancktelow, N., Seward, D., 2000. Cretaceous to Neogene cooling and exhumation history of the Oetztal–Stubai basement complex, eastern Alps: a structural and fission track study. Tectonics 19, 905–918.
Goguel, J., 1978. Scale-dependent rockslide mechanisms, with emphasis on the role of pore fluid vaporization. In: Voight, B. (Ed.), Rockslides and Avalanches, 1 Natural Phenomena: Dev. Geotech. Eng., 14A, pp. 693–705.
Hewitt, K., 1999. Quaternary moraines vs. catastrophic rock avalanches in the Karakoram Himalaya, northern Pakistan. Quaternary Research 51, 220–237.
Hungr, O., Evans, S.G., 2004. Entrainment of debris in rock avalanches; an analysis of a long run-out mechanism. Bulletin of the Geological Society of America 116, 1240–1252.
Imre, B., Laue, J., Springmann, S.M., 2010. Fractal fragmentation of rocks within sturzstroms: imsight derived from physical experiments within the ETH geotechnical drum centrifuge. Granular Matter 12, 267–285.
Ivy-Ochs, S., Synal, H.-A., Roth, C., Schaller, M., 2004. Initial results from isotope dilution for Cl and ^{36}Cl measurements at the PSI/ETH Zurich AMS facility. Nuclear Instruments and Methods in Physics Research Section B: Beam Interactions with Materials and Atoms 223–224, 623–627.
Ivy-Ochs, S., Kerschner, H., Kubik, P.W., Schlüchter, Ch., 2006. Glacier response in the European Alps to Heinrich Event 1 cooling: the Gschnitz stadial. Journal of Quaternary Science 21, 115–130.
Ivy-Ochs, S., Poschinger, A.v., Synal, H.-A., Maisch, M., 2009. Surface exposure dating of the Flims landslide, Graubünden, Switzerland. Geomorphology 103, 104–112.
Kerschner, H., 1978. Untersuchungen zum Daun- und Egesenstadium in Nordtirol und Graubünden (methodische Überlegungen). Geographische Jahresbericht aus Österreich 36, 26–49.

Kerschner, H., Hertl, A., Gross, G., Ivy-Ochs, S., Kubik, P.W., 2006. Surface exposure dating of moraines in the Kromer valley (Silvretta Mountains, Austria)-evidence for glacial response to the 8.2 ka event in the Eastern Alps? The Holocene 16, 7–15.

Klitgaard-Kristensen, D., Sejrup, H.P., Haflidason, H., Johnson, S., Spurk, M., 1998. A regional 8200 cal.yr BP cooling event in northwest Europe, induced by final stages of the Laurentide ice-sheet glaciation. Journal of Quaternary Science 13, 165–169.

Liu, B., Phillips, F.M., Fabryka-Martin, J.T., Fowler, M.M., Stone, W.D., 1994. Cosmogenic ^{36}Cl accumulation in unstable landforms: 1. Effects of the thermal neutron distribution. Water Resources Research 30, 3115–3125.

Louge, M.Y., Keast, S.C., 2001. On dense granular flows down flat frictional inclines. Physics of Fluids 13, 1213–1233.

Magiera, J., 2000. Bericht 1999 über geologische Aufnahmen im Quartär des Obernbergtals auf Blatt 148 Brenner. Jahrbuch der Geologischen Bundesanstalt 142/3 (301–302 and 364–365).

Magny, M., Begeot, C., Guiot, J., Marguet, A., Billaud, Y., 2003. Reconstruction and palaeoclimatic interpretation of mid-Holocene vegetation and lake-level changes at Saint-Jorioz, Lake Annecy, French Pre-Alps. The Holocene 13, 265–275.

Major, J.J., 1997. Depositional processes in large-scale debris-flow experiments. Journal of Geology 105, 345–366.

Melosh, H.J., 1986. The physics of very large landslides. Acta Mechanica 64, 89–99.

Melosh, H.J., 1996. Dynamical weakening of faults by acoustic fluidization. Nature 379, 601–606.

Paschinger, H., 1953. Bergsturz und spätglaziale Moränen im Obernberger Tal (Brenner Tirol). Zeitschrift für Gletscherkunde und Glazialgeologie 2, 312–316.

Phillips, F.M., Stone, W.D., Fabryka-Martin, J.T., 2001. An improved approach to calculating low-energy cosmic-ray neutron fluxes near the land/atmosphere interface. Chemical Geology 175 (3–4), 689–701.

Pollet, N., Schneider, J.-L.M., 2004. Dynamic disintegration processes accompanying transport of the Holocene Flims sturzstrom (Swiss Alps). Earth and Planetary Science Letters 221, 433–448.

Prasad, S., Witt, A., Kienel, U., Dulski, P., Bauer, E., Yancheva, G., 2009. The 8.2 ka event: evidence for seasonal differences and the rate of climate change in western Europe. Global and Plantary Change 67, 218–226.

Reimer, P.J., Baillie, M.G.L., Bard, E., Bayliss, A., Beck, J.W., Blackwell, P.G., Bronk Ramsey, C., Buck, C.E., Burr, G.S., Edwards, R.L., Friedrich, M., Grootes, P.M., Guilderson, T.P., Hajdas, I., Heaton, T.J., Hogg, A.G., Hughen, K.A., Kaiser, K.F., Kromer, B., McCormac, F.G., Manning, S.W., Reimer, R.W., Richards, D.A., Southon, J.R., Talamo, S., Turney, C.S.M., van der Plicht, J., Weyhenmeyer, C.E., 2009. IntCal09 and Marine09 radiocarbon age calibration curves, 0–50,000 years cal BP. Radiocarbon 51, 1111–1150.

Reiser, M.K., Scheiber, Th., Fügenschuh, B., Burger, U., 2010. Hydrological characterisation of Lake Obernberg, Brenner pass area, Tyrol. Austrian Journal of Earth Sciences 103, 43–57.

Reiter, F., Lenhardt, W.A., Decker, K., Brandner, R., 2003. Aktive Tektonik und Seismizität im Bereich Wipptal-Inntal. — Andauern der lateralen Extrusion? In: Geologische Bundesanstalt (Ed.), Arbeitstagung der Geologischen Bundesanstalt "Brenner", Trins, Geologische Kartenblätter 148 Brenner und 175 Sterzing, pp. 179–184.

Reitner, J.M., 2007. Glacial dynamics at the beginning of Termination I in the Eastern Alps and their stratigraphic implications. Quaternary International 164–165, 64–84.

Rockenschaub, M., Brandner, R., Burger, U., Decker, K., Kirschner, H., Maurer, C., Millen, B., Poscher, G., Prager, C., Reiter, F., 2003. Umwelttektonik der Östlichen Stubaier Alpen und des Wipptals. Unpublished Final Report of the Project TC 12, 228 pp.

Rohling, E.J., Pälike, H., 2005. Centennial-scale climate cooling with a sudden cold event around 8,200 years ago. Nature 434, 975–979.

Sartori, M., Baillifard, F., Jaboyedoff, M., Rouiller, J.-D., 2003. Kinematics of the 1991 Randa rockslides (Valais, Switzerland). Natural Hazards and Earth System Sciences 3, 423–433.

Schmid, S.M., Fügenshuh, B., Kissling, E., Schuster, R., 2004. Tectonic map and overall architecture of the Alpine orogen. Eclogae Geologicae Helvetiae 97, 93–117.

Shugar, D.H., Clague, J.J., 2011. The sedimentology and geomorphology of rock avalanche deposits on glaciers. Sedimentology 58, 1763–1783.

Stone, J.O.H., 2000. Air pressure and cosmogenic isotope production. Journal of Geophysical Research, B: Solid Earth 105 (B10), 23753–23759.

Stone, J.O.H., Allan, G., Fifield, L., Cresswell, R., 1996. Cosmogenic chlorine-36 from calcium spallation. Geochimica et Cosmochimica Acta 60, 679–692.

Stone, J.O.H., Evans, J.M., Fifield, L.K., Allan, G.L., Cresswell, R.G., 1998. Cosmogenic chlorine-36 production in calcite by muons. Geochimica et Cosmochimica Acta 62, 433–454.

Synal, H.-A., Bonani, G., Döbeli, M., Ender, R.M., Gartenmann, P., Kubik, P.W., Schnabel, Ch., Suter, M., 1997. Status report of the PSI/ETH AMS facility. Nuclear Instruments and Methods in Physics Research Section B: Beam Interactions with Materials and Atoms 123, 62–68.

Van Husen, D., 1987. Die Ostalpen in den Eiszeiten. Geologische Bundesanstalt, Vienna, p. 24, 1 map.

Van Husen, D., 1997. LGM and Late glacial fluctuations in the Eastern Alps. Quaternary International 38 (39), 109–118.

Van Husen, D., 2004. Quaternary glaciations in Austria. In: Ehlers, J., Gibbard, P.L. (Eds.), Quaternary Glaciations—Extent and Chronology. : Developments in Quaternary Science, 2. Elsevier, Amsterdam, pp. 1–13.

Wastl, M., 2007. Zur Geomorphologie des hinteren Obernbergtals. In: Innsbrucker Geographische Gesellschaft (Ed.), Alpine Kulturlandschaft im Wandel. Hugo Penz zum 65. Geburtstag, pp. 146–153.

Zambrano, O.M., 2008. Large rock avalanches: a kinematic model. Geotechnical and Geological Engineering 26, 283–287.